



# Cationic surface functionalization of cellulose nanocrystals and its effect on the mechanical properties of polyamide 6 thin films

Abdelhaq Benkaddour · Casey Rusin · Eyup Can Demir · Cagri Ayranci · Mark McDermott

Received: 22 November 2022 / Accepted: 9 June 2023 / Published online: 29 June 2023  
© The Author(s), under exclusive licence to Springer Nature B.V. 2023

**Abstract** The interfacial interaction between cellulose nanocrystals (CNCs) and polymeric matrices is important in the development of reinforced polymer nanocomposites. In this work, spin-coated polyamide 6 thin films were reinforced with CNCs and their effects on the mechanical properties are evaluated. Interfacial interactions were improved by using two CNCs surface modifications: (1) TEMPO-oxidation and (2) cationic adsorption of cetrimonium bromide (CTAB). The nanomaterials were characterized using infrared spectroscopy, x-ray photoelectron spectroscopy, zeta potential, CHNS elemental analysis and x-ray diffraction. The mechanical testing results indicated that the tensile modulus and strength of the films slightly increased by adding 2.5 wt.% of

unmodified CNCs and the increase was more noticeable at 5 wt.%. When CTAB was adsorbed unmodified CNCs, no mechanical improvement was observed at 1 and 2.5 wt.%, but an obvious increase of elastic modulus (32%) and tensile strength (71%) was seen at 5 wt.%. Further enhancement of the mechanical properties occurred when TEMPO oxidized CNCs was used as reinforcing agent due to the increase of negative charges induced by the oxidation. At 5 wt.% of TEMPO-oxidized CNCs, an improvement of 131% and 174% was observed in elastic modulus and tensile strength, respectively. Finally, when CTAB was adsorbed to TEMPO-oxidized CNCs, an additional mechanical amelioration was noticed. With only 1 wt.% loading, an increase of 142% and 131% was obtained in elastic modulus and tensile strength, respectively.

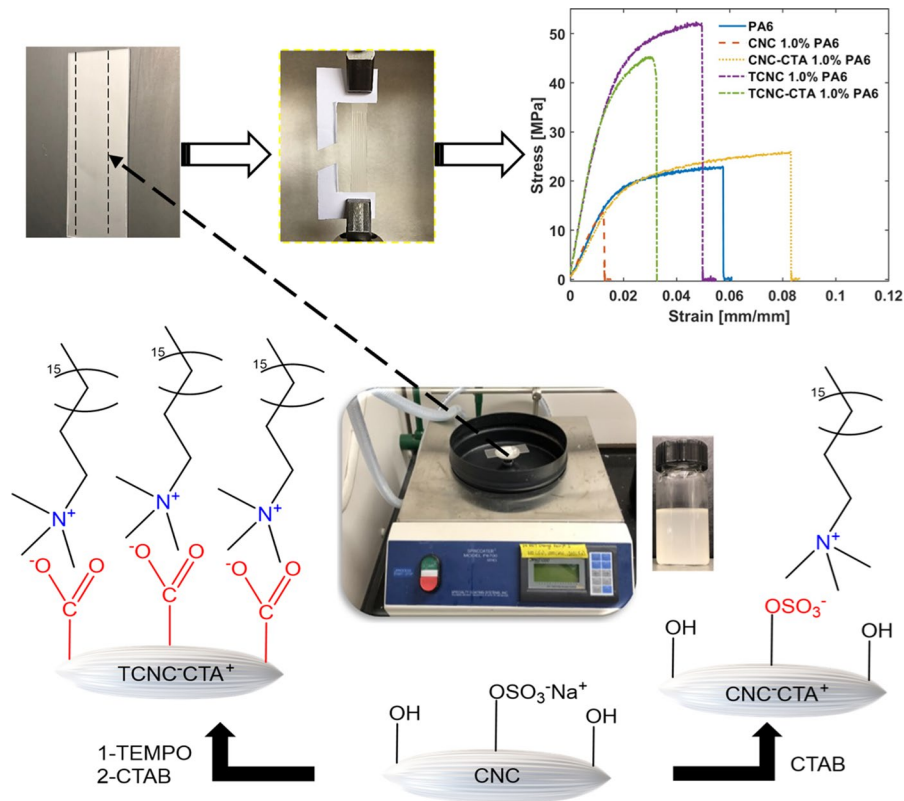
**Supplementary Information** The online version contains supplementary material available at <https://doi.org/10.1007/s10570-023-05313-6>.

A. Benkaddour · C. Rusin · M. McDermott (✉)  
Department of Chemistry, University of Alberta,  
Edmonton, AB, Canada  
e-mail: mark.mcdermott@ualberta.ca

A. Benkaddour · E. C. Demir · C. Ayranci (✉)  
Department of Mechanical Engineering, University  
of Alberta, Edmonton, AB, Canada  
e-mail: cayranci@ualberta.ca

A. Benkaddour  
Sustainable Materials Research Center (SusMat-RC),  
Mohammed VI Polytechnic University (UM6P),  
43150 Ben Guerir, Morocco

## Graphical abstract



**Keywords** Cellulose nanocrystals · Cetrimonium bromide · Polyamide 6/nylon 6 · Mechanical properties · Thin films

## Introduction

Nanomaterials are commonly used as reinforcing agents due to the enhanced mechanical properties they offer at low concentrations (Yao et al. 2014). One promising nanomaterial is cellulose nanocrystals (CNCs) owing to its biodegradability, reactive and high surface area ( $150\text{--}600\text{ m}^2\text{g}^{-1}$ ) (Gardner et al. 2008; Sehaqui et al. 2011), high aspect ratio, low cost and high mechanical stiffness and strength (Eichhorn 2011; Saito et al. 2013). CNCs are prominently used in biomedical (Lin et al. 2012), wastewater treatment, energy, electronic (Chakrabarty and Teramoto 2018), automotive, aerospace and construction

industries (Karimi 2017). CNCs are also commonly used as an additive in polymer composites to provide improved mechanical properties (Kalia et al. 2009). The increase in mechanical performance is dependent on the compatibility between CNCs and the polymeric matrix (Baiardo et al. 2002; Gradwell et al. 2004). CNCs has a tendency to form hydrogen bonds between adjacent crystals (self-aggregation) due to its hydrophilic nature, thus reducing the interaction and compatibility with hydrophobic molecules and non-aqueous media (Baiardo et al. 2002). Moreover, most CNCs are commonly processed using sulfuric acid hydrolysis, which results in negatively charged surface sulfate half-ester groups. These groups are responsible for the low thermal stability of CNCs (Roman and Winter 2004; Lin and Dufresne 2014), and limits CNC-polymer nanocomposite preparation to wet processing methods due to degradation at the high processing temperatures (Ben Azouz et al. 2012).

Polyamide 6 (PA6) is a widely used polymer to produce fibers and engineered materials. Despite PA6's commercial popularity, CNC reinforced PA6 has not been utilized in the industry. Even academic studies investigating CNC reinforced PA6 nanocomposites is very limited in the literature. Yousefian and Rodrigue (2014) compounded spray-dried CNCs (3 wt.%) with PA6 using extrusion at 220 °C, and they reported 23% and 11% increase in tensile modulus and tensile strength, respectively. Corrêa et al. (2014) showed that freeze-dried CNCs coated by PA6 in formic acid solution improved the thermal stability. In their work, CNC reinforced PA6 nanocomposites were obtained by extrusion and subsequent injection molding. The addition of 1 wt.% CNCs to PA6 increased the elastic modulus by 45%, while the tensile strength slightly decreased. Another method used to prepare CNC reinforced nanocomposites is solvent casting. Qua and Hornsby (2011) solvent cast a suspension of unmodified CNCs (5 wt.%) and PA6 in formic acid to prepare PA6/CNC nanocomposite films. An improvement of 28% and 100% was observed in elastic modulus and tensile strength, respectively. While melt processing and solvent casting techniques show slight improvements in the mechanical properties, the distribution of CNCs in PA6 is poor and remains a limiting factor for mechanical strength improvement (Peng et al. 2015).

CNC surface functionalization can change the hydrophilicity of the nanomaterial and prevent agglomeration when drying. There are many chemical and physical CNC modifications reported in the literature, including acetylation (Çetin et al. 2009), esterification (Bendahou et al. 2015), etherification (Liu et al. 2017) and polymer grafting (Ljungberg et al. 2005; Yi et al. 2008; Cao et al. 2009; Morandi et al. 2009). These modifications that involve the covalent bonding of molecules to the CNC surface often require the use of organic solvents that pose disposal or recycle issues. Alternatively, ionic adsorption of surfactants to CNCs is straightforward and an environmentally friendly process (Salajková et al. 2012; Heera and D 2014; Kaboorani and Riedl 2015; Nagalakshmaiah et al. 2016; Rehman et al. 2017; Yalcinkaya et al. 2017; Liu et al. 2017; Yin et al. 2018). The ionic adsorption of surfactants to unmodified CNCs containing sulfate-half ester groups is relatively poor and unstable due to weak surface interactions (Yin et al. 2018). The surface interactions can be

improved by subjecting CNCs to 2,2,6,6-tetramethylpiperidine 1-oxy (TEMPO) oxidation (TCNCs). This process converts the primary C6 hydroxyl groups into C6 carboxylate groups (Patiño-Masó et al. 2019), thus increasing electrostatic interactions with cationic surfactants.

Herein, we implement an eco-friendly procedure to surface modify CNCs with cetrimonium bromide (CTAB) in aqueous medium through electrostatic adsorption. Two modifications were performed: (1) TEMPO-oxidation of CNCs (TCNCs) and (2) cationic adsorption of CTAB onto CNCs and TCNCs. Both of these modification steps are performed in aqueous media that are potentially more attractive in industrial applications. Unmodified and modified PA6/CNCs nanocomposite thin films were produced using spin-coating. Spin-coating has not been extensively used to produce CNC reinforced PA6 nanocomposite even though it is a superior technique compared to solvent casting due its ability to reproducibly make specimens with controlled and homogeneous thicknesses. The effect of CNC surface functionalization on the mechanical properties of the PA6 thin films was investigated.

## Experimental

### Materials

The CNCs were received from InnoTech Alberta, and it was produced from commercially bleached softwood Kraft pulp using sulfuric acid hydrolysis. 2,2,6,6-tetramethylpiperidine 1-oxy (98%, TEMPO), sodium bromide ( $\geq 99\%$ , NaBr), sodium hypochlorite (13%, NaOCl), cetrimonium bromide (98%, CTAB) and formic acid (98%, FA) were purchased from Sigma Aldrich and used as received. PA6 (Nylene 600) was purchased from Nylene Inc. USA.

### Preparation of TEMPO-oxidized CNCs (TCNCs)

TEMPO-oxidation was performed based on previously published literature (Saito et al. 2006). CNCs (5 g) were dispersed in deionized water (500 mL) along with TEMPO (0.1 mmol/g of CNCs) and NaBr (3 mmol/g of CNCs). The reaction was initiated with the addition of NaOCl (2.5 mmol/g CNCs) at room temperature under magnetic stirring. The reaction pH

was maintained at 10.5 using 0.5 M NaOH. When the solution pH no longer decreased, the reaction was stopped with the addition of ethanol (5 mL). The solution pH was adjusted to 7 using 0.5 M HCl. TCNCs were dialyzed against deionized water followed by freeze-drying.

### Cationic coupling of CTAB to CNCs and TCNCs

Figure 1 shows the modification of CNCs and TCNCs with CTAB. The modification was based on previous literature (Nagalakshmaiah et al. 2016). CNCs (5 g) was dispersed in aqueous medium (1 wt.%) and the pH was adjusted to 10 using NaOH. Aqueous solution of CTAB (10 wt.%) was added slowly to the CNCs dispersion and mixed at 40 °C for 3 h. The mixture was then stirred at room temperature and dialyzed against deionized water for 15 days to remove excess unreacted CTAB and NaBr. The modified CNCs (CNCs<sup>-CTA<sup>+</sup></sup>) were freeze-dried before incorporation into PA6. The same procedure was used for functionalization of TCNCs (TCNCs<sup>-CTA<sup>+</sup></sup>).

### Preparation of spin-coated PA6 nanocomposite thin films

PA6 nanocomposite films were prepared using spin-coating. A rectangular (25 mm × 75 mm) glass substrate was spin-coated with 2 mL of suspension. The initial rotation speed was 2000 rpm for 15 s and then brought to 3000 rpm for 30 s. The substrates were allowed to

rest for 5 min to allow for excess solvent to evaporate. The solvent used was FA and PA6 was mixed with 1, 2.5 and 5 wt.% unmodified and modified CNCs. Film thickness was determined to be in the range of 10–15 μm using a caliper.

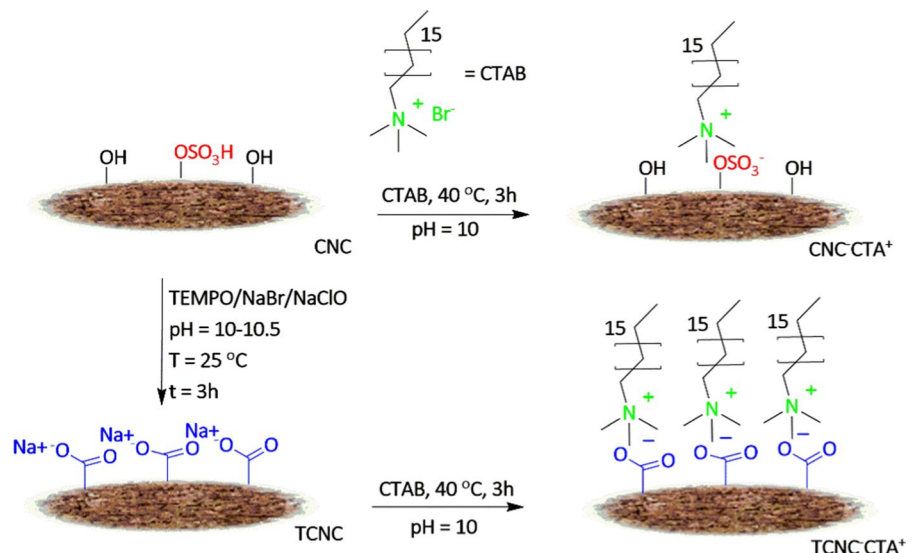
### Characterization

The surface charge density of the CNCs was measured using a Malvern Zetasizer Nano-ZS. The value for each sample is the average of 5 repetitions.

The sulfate half-ester content of unmodified CNCs was determined using a conductometric titration using a Meter Star, A212 conductivity meter. A 2 wt.% solution of CNCs was mixed with Dowex Marathon<sup>TM</sup> C hydrogen form resin several times over 8 h. Before use, the resin was rinsed and filtered several times until the filtrate was clear and of neutral pH. After protonation of CNCs sulfate half-ester groups, the remaining CNCs in solution was determined as 1.20 ± 0.02 wt.%. The CNCs (5 mL) was diluted with DI water (100 mL) and mixed with NaCl (2 mL, 100 mM). The initial pH of the solution was approximately 3.5 and was titrated to a pH of 10 using NaOH (15 mM) at 100 μL intervals. The sulfate half-ester content was determined using Eq. 1 (Beck et al. 2015)

$$\text{OSO}_3\text{H} \left( \frac{\text{mmol}}{\text{g}} \right) = \frac{[\text{C}_{\text{NaOH}}] \times V_{\text{NaOH}}}{m_{\text{CNCs}}} \quad (1)$$

**Fig. 1** Reaction scheme for the modification of CNCs



$C_{\text{NaOH}}$  is the concentration of NaOH,  $V_{\text{NaOH}}$  is the volume of NaOH consumed in the titration and  $m_{\text{CNCs}}$  is the mass of CNCs. The titration was performed in triplicates.

The carboxyl content of TCNCs was determined using a similar titration. Freeze-dried TCNCs (0.032 g) was mixed with DI water (100 mL), NaCl (2 mL, 100 mM) and HCl (2.5 mL, 40 mM) for 3 h to ensure protonation of carboxylic acid groups. The initial pH of the slurry was 2.8 and titrated with NaOH (15 mM) at 100  $\mu\text{L}$  intervals until a pH of 10.5. The carboxyl content was determined using Eq. 2 (Benkaddour et al. 2013a).

$$\text{COOH}(\text{mmol/g}) = \frac{C_{\text{NaOH}}(V_2 - V_1)}{m_{\text{CNC}}} \quad (2)$$

$V_1$  and  $V_2$  are the equivalent volumes of added NaOH solution (mL) needed to neutralize the free protons from HCl and those bound by the carboxylic groups, respectively. The degree of oxidation (DO) is given using Eq. 3 (Benkaddour et al. 2013b)

$$\text{DO} = \frac{162 \left( \frac{\text{g}}{\text{mol}} \right) \times \text{COOH} \left( \frac{\text{mmol}}{\text{g}} \right) \times 10^{-3}}{1 - 36 \times \text{COOH} \left( \frac{\text{mmol}}{\text{g}} \right) \times 10^{-3}} \quad (3)$$

where 36 is the difference between the molecular weight of the anhydroglucose unit and that of the sodium salt of a glucuronic acid and 162 is the molecular weight of one anhydroglucose unit.

Fourier Transform Infrared (FTIR) spectra were collected using Nicolet 8700 FTIR spectrometer. Dried sample (1 mg) and KBr (100 mg) powder were ground together using a mortar and pestle and pressed to form discs. A total of 32 scans were taken per sample with a resolution of 4  $\text{cm}^{-1}$  (4000–400  $\text{cm}^{-1}$ ).

X-ray photoelectron spectroscopy measurements were performed with a Kratos Ultra electron spectrometer using a monochromatic Al  $K\alpha$  ( $h\nu = 1486.6$  eV) X-ray source (Kratos Analytical, Manchester, UK). The collected data were analyzed using CASA XPS version 2.3.

The degree of substitution (DS) of  $\text{CNCs}^{-\text{CTA}^+}$  and  $\text{TCNCs}^{-\text{CTA}^+}$  was measured using the percentage of nitrogen (%N). The %N was measured using a Thermo Flash 2000 Elemental Analyzer CHNS and Oxygen. The DS of  $\text{CNCs}^{-\text{CTA}^+}$  and

$\text{TCNCs}^{-\text{CTA}^+}$  were calculated based on the Eq. 4 (Zainuddin et al. 2017).

$$\text{DS} = \frac{162 \times \%N/100}{14 - 364.45 \times \%N/100} \quad (4)$$

XRD analysis were performed on dried unmodified and modified CNCs nanomaterials. Measurements were performed with a diffractometer (Rigaku Ultima IV) operated at 40 kV and 44 mA. The  $2\theta$  range was from  $10^\circ$  to  $50^\circ$  using a counting time 120 s with a step size of  $0.05^\circ$  and Cu  $K\alpha$  radiation ( $\lambda = 1.5418 \text{ \AA}$ ).

Transmission electron microscopy (TEM) images were collected using Philips 410 transmission electron microscope at 100 kV to observe the morphology of pure CNCs and modified CNCs.

Mechanical testing was performed using a TA instruments ElectroForce 3200 with a load cell of maximum 10 N capacity. The sample dimensions had a width of 10 mm and a length of 50 mm. The specimens were stored in desiccators containing silica gel after production until testing. All measurements were carried out at room temperature with a crosshead speed of 0.083 mm/s (0.1 mm/min). The reported values are the average of 5 repetitions.

## Results and discussion

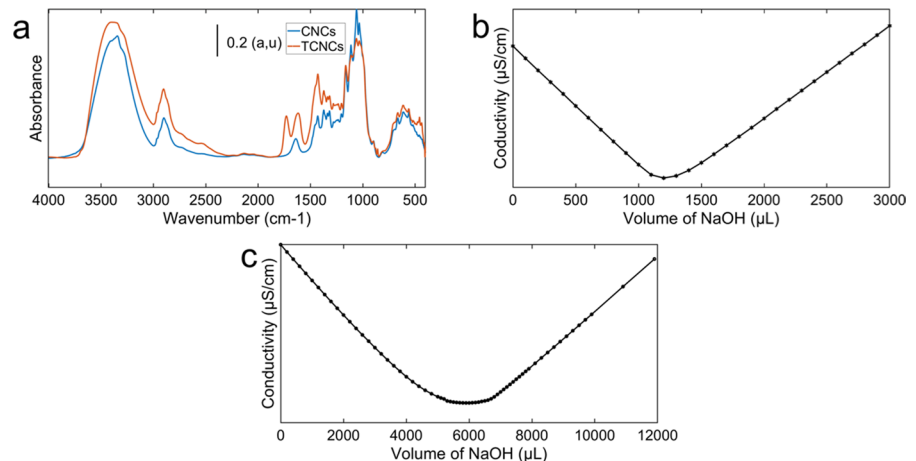
### Characterization of CNCs and TCNCs

First, CNCs was TEMPO-oxidized to obtain carboxylated CNCs (TCNCs). FTIR spectroscopy was used to characterize and confirm surface modification. Figure 2a shows the FTIR spectra of CNCs and TCNCs. Both the CNCs and TCNCs spectra show cellulose bands at 3344  $\text{cm}^{-1}$ , 2893  $\text{cm}^{-1}$ , 1428  $\text{cm}^{-1}$  and 1059  $\text{cm}^{-1}$  that are attributed to  $\nu$  (O–H),  $\nu$  (C–H),  $\delta$  (C–H) and  $\nu$  (C–O), respectively (Abou-Zeid et al. 2015). In the CNCs spectrum, the band at 1639  $\text{cm}^{-1}$  is from  $\delta$  (O–H) due to absorbed water (Abou-Zeid et al. 2015). Following CNCs oxidation, two new bands are observed at 1730  $\text{cm}^{-1}$  and 1610  $\text{cm}^{-1}$  due to  $\nu$  (C=O) and  $\nu_{\text{as}}$  (COO $^-$ ), respectively ( $\sim$ pH 4) (Yin et al. 2018).

The sulfate half-ester and carboxylate content on CNCs and TCNCs were determined using an electric conductivity titration. Figure 2b, c are conductometric titration plots used to determine the sulfate half-ester



**Fig. 2** **a** FTIR spectra of CNCs and TCNCs. Determination of **b** sulfate half-ester groups on CNCs and **c** carboxylate groups on TCNCs using an electric conductivity titration



and carboxylate content, respectively. The sulfate half-ester content on unmodified CNCs was determined as  $0.295 \pm 0.002$  mmol/g, which falls within previously reported values of 0.093–0.311 mmol/g (Jordan et al. 2019). After oxidation, the carboxylate content was determined to be  $1.01 \pm 0.03$  mmol/g., which also falls within previously reported values of 0.38 and 1.75 mmol/g (Liimatainen et al. 2012). The degree of oxidation was calculated as 0.169, similar to those reported in the literature (Saito et al. 2006).

The surface charge of CNCs and TCNCs were determined using  $\zeta$ -potential measurements. The surface charge of CNCs was measured as  $-45 \pm 1$  mV (pH 6.5–7), which is due to the negatively charged sulfate half-ester groups introduced with sulfuric acid hydrolysis (Rehman et al. 2017). After TEMPO oxidation, the  $\zeta$ -potential of TCNCs was measured at  $-60 \pm 2$  mV (pH 6.5–7). The increase in surface charge observed is due to the formation of negatively charged carboxylate groups during TEMPO-oxidation.

#### Cationic adsorption of CTAB to CNCs and TCNCs

The surface modification of CNCs and TCNCs with CTAB was monitored with FTIR spectroscopy. Figure 3a shows the FTIR spectra for CNCs<sup>-</sup>CTA<sup>+</sup> and TCNCs<sup>-</sup>CTA<sup>+</sup>. Both spectra showed the characteristic cellulose features, however, the bands in TCNCs<sup>-</sup>CTA<sup>+</sup> are more pronounced due to stronger electrostatic interaction between TCNCs and CTAB. In both spectra, the bands at 2852 and 2924 cm<sup>-1</sup> correspond to  $\nu_{as}$  and  $\nu_s$  (C–H) from the alkyl chains

in CTAB, (Salajková et al. 2012). The weak intensity band at 1480 cm<sup>-1</sup> corresponds to the trimethyl groups of the quaternary ammonium (Heera and D 2014). This band is not as pronounced in CNCs<sup>-</sup>CTA<sup>+</sup> due to weaker electrostatic interaction between the sulfate half-ester and the quaternary ammonium group. The decrease in the  $\nu$  (O–H) band at 3344 cm<sup>-1</sup> is attributed to the adsorption of CTAB to the CNCs and TCNCs.

The cationic adsorption of CTAB resulted in a change in the surface charge of CNCs and TCNCs. The  $\zeta$ -potential values after the adsorption of CTAB were measured as  $-15.6 \pm 0.8$  mV and  $-11.0 \pm 0.6$  mV for CNCs<sup>-</sup>CTA<sup>+</sup> and TCNCs<sup>-</sup>CTA<sup>+</sup>, respectively. The increase in surface charge is a result of the cationic adsorption of CTAB to the sulfate half-ester and carboxylate groups thus neutralizing the respective negatively charged surface groups.

The reinforcement effect of CNCs in nanocomposites is correlated to the crystalline structure of CNCs (Heera and D 2014). When CNCs are modified, it is important to maintain the crystalline structure in order to retain the reinforcing properties. XRD analysis was used to investigate the impact of CTAB adsorption on the crystalline structure of CNCs. Figure 3b shows the diffraction patterns of unmodified, TCNCs, and modified CNCs (CNC<sup>-</sup>CTA<sup>+</sup> and TCNC<sup>-</sup>CTA<sup>+</sup>). The peaks that appear at 14.6°, 16.3°, 20.5°, 22.7° and 34.5° correspond to the  $\bar{1}10$ , 110, a mixture of 012 and 102, 200, and 004 reflection planes of cellulose I $\beta$  (French 2014). These peaks appear in both the CNCs and TCNCs samples as

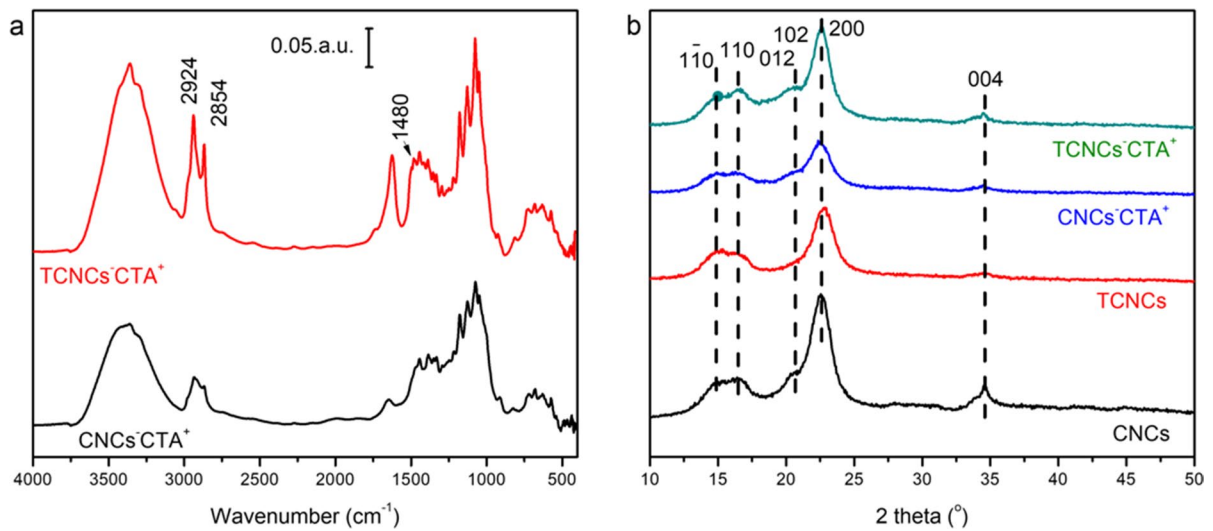


**Fig. 3** **a** FTIR spectra of  $\text{CNC}^-\text{CTA}^+$  and  $\text{TCNC}^-\text{CTA}^+$ . **b** XRD analysis of unmodified and modified CNCs and TCNCs

well as after surface modification with CTAB, therefore, TEMPO-oxidation has no effect on the crystal structure of CNCs (Isogai et al. 2011). Moreover, no change in crystal structure after the modification with CTAB suggests that this also has no effect on the crystal structure.

The coupling of CTAB to CNCs and TCNCs was thoroughly investigated using CHNS elemental analysis and is shown in Table 1. The coupling yield of CTAB with CNCs and TCNCs was determined gravimetrically as 22 wt.% and 65 wt.% for  $\text{CNC}^-\text{CTA}^+$  and  $\text{TCNC}^-\text{CTA}^+$ , respectively. Notably, the %N for CNCs and TCNCs is  $<0.2\%$ , while after CTAB adsorption the %N increases to  $0.318 \pm 0.004$  and  $1.317 \pm 0.002\%$  for  $\text{CNC}^-\text{CTA}^+$  and  $\text{TCNC}^-\text{CTA}^+$ , respectively. The %N content increases by a factor of  $\sim 4$  after TCNCs is modified with CTAB. The difference in carboxylate content and sulfate half-ester content is approximately 3.4 times [ $1.01$  (mmol/kg)/ $0.295$  (mmol/kg)], which relates closely to the %N content increase. Using the information provided

by CHNS, the degree of substitution of  $\text{CNC}^-\text{CTA}^+$  and  $\text{TCNC}^-\text{CTA}^+$  was calculated as 0.04 and 0.23, respectively.

The cationic adsorption of CTAB onto CNCs and TCNCs was investigated using XPS analysis. The survey spectra of the samples are shown in SI Fig. 1. The main chemical components from the survey spectra are C and O, and the results are tabulated in SI Table 1. A slight decrease in the O/C ratio from 0.66 to 0.61 were observed when CNCs were modified with CTAB, while the decrease in the O/C ratio was more pronounced when TCNCs were modified (0.66–0.39). This change in the O/C indicates the adsorption of CTAB to the surface of TCNCs due to the addition of the carbon-rich CTAB group, thus lowering the O/C ratio.

The C 1s high resolution XPS peak can be used to describe the chemical environment of cellulosic materials. Figure 4 shows the deconvolutions of the C 1s for each sample. The results were tabulated and listed in SI Table 1. Figure 4a shows the C 1s

**Table 1** CHNS elemental analysis of unmodified and modified CNCs/TCNCs

Sample	%N	%C	%H	%S
CNCs	$<0.2$	$40.916 \pm 0.005$	$6.10 \pm 0.02$	$0.75 \pm 0.01$
TCNCs	$<0.2$	$37.389 \pm 0.002$	$5.4 \pm 0.1$	$0.54 \pm 0.02$
$\text{CNC}^-\text{CTA}^+$	$0.318 \pm 0.004$	$42.3 \pm 0.6$	$6.4 \pm 0.3$	$0.65 \pm 0.02$
$\text{TCNC}^-\text{CTA}^+$	$1.317 \pm 0.002$	$51.69 \pm 0.01$	$8.033 \pm 0.002$	$0.54 \pm 0.02$

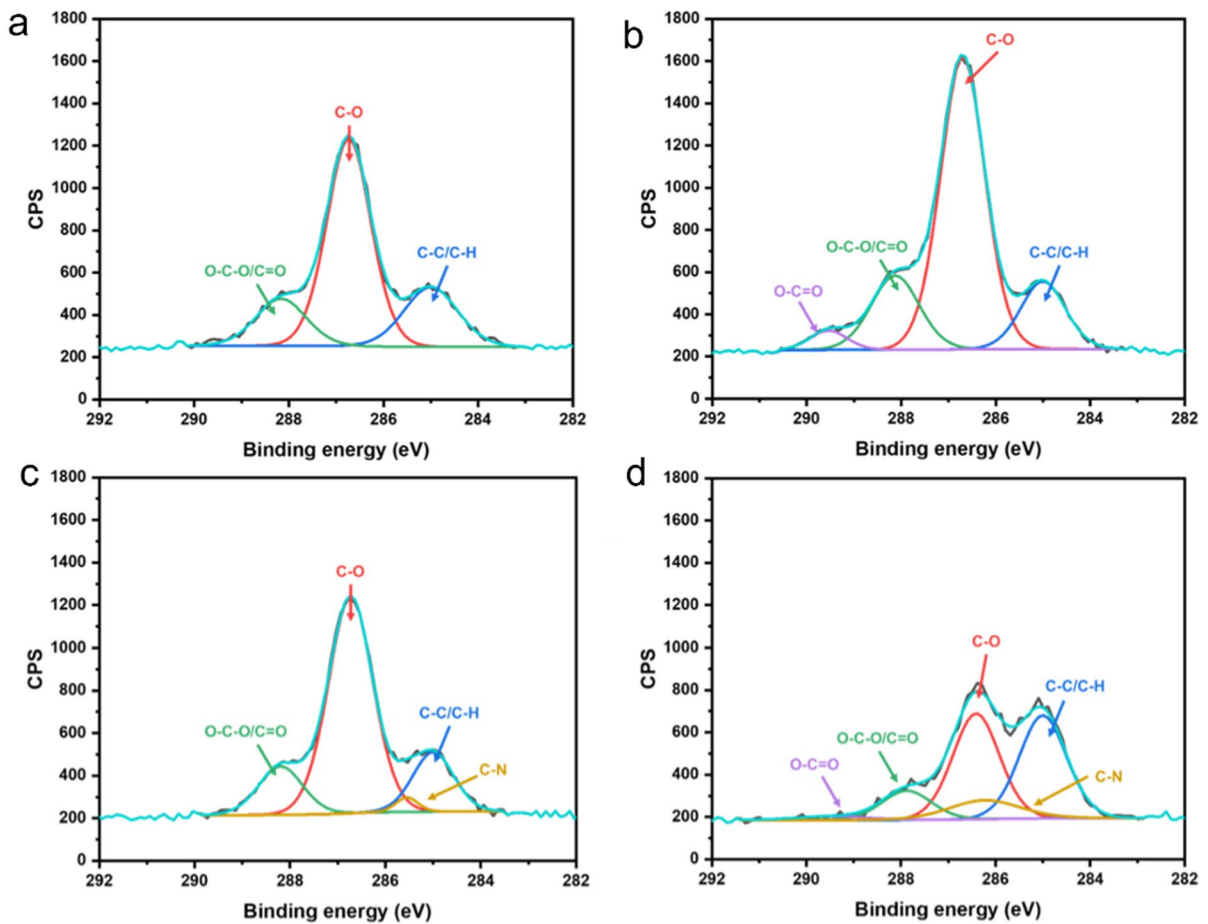


**Fig. 4** High resolution XPS of C 1s deconvolution for **a** CNCs, **b** TCNCs, **c** CNCs<sup>-</sup>CTA<sup>+</sup> and **d** TCNCs<sup>-</sup>CTA<sup>+</sup>

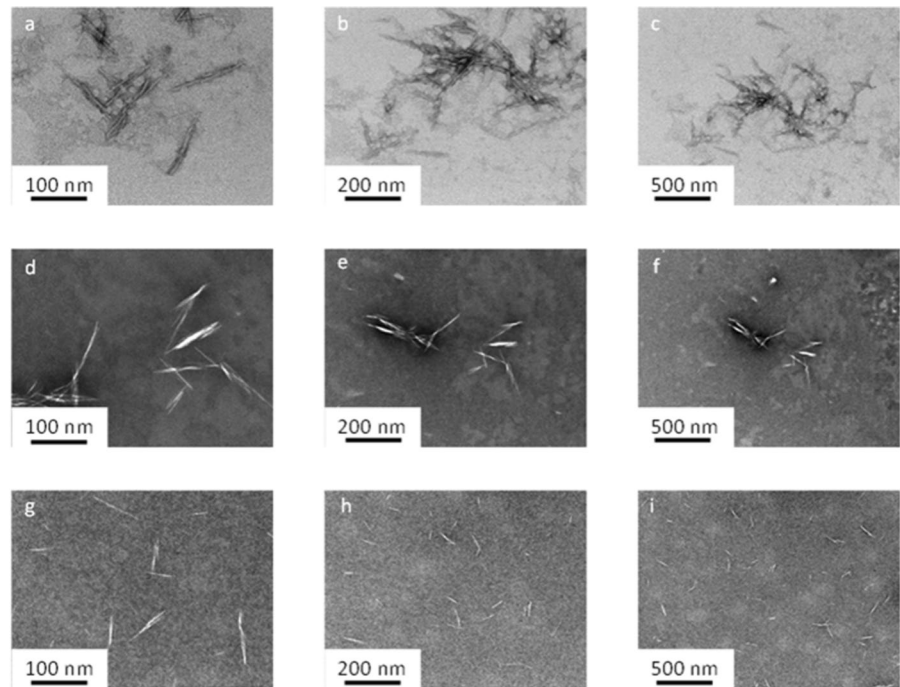
high resolution of CNCs. It displays three bonds: C–C/C–H, C–O and O–C–O. These correspond well with what has been observed in the literature for sulfuric acid hydrolysis treated CNCs (Khili et al. 2019). An additional bond, O–C=O, is commonly observed in low quantities for CNCs (Kaboarani and Riedl 2015), however, this was not observed in our sample. In Fig. 4b, a new component appeared following CNCs oxidation labelled as O–C=O from the presence of the carboxylic acid groups on TCNCs (Bendahou et al. 2015). As shown in Fig. 4c, the adsorption of CTAB onto CNCs was observed by the emergence of a C–N peak due to the quaternary ammonium of CTAB (Kaboarani and Riedl 2015). The C–N peak increases by a factor of 4.7 when CTAB was adsorbed to TCNCs (Fig. 4d). This is in agreement to the results observed for CHNS elemental analysis.

Transmission electron microscopy of unmodified and modified CNCs

The structural morphology of modified and unmodified CNCs was investigated by means of TEM. The TEM images of CNCs, CNC<sup>-</sup>CTA<sup>+</sup>, TCNCs and TCNC<sup>-</sup>CTA<sup>+</sup> are displayed in Fig. 5. As shown in Fig. 5a–c, CNCs are highly hydrophilic and prone to form agglomerates due to interparticle hydrogen bonding. Therefore, to avoid agglomerations, it is necessary to conduct the physical modification with the cationic surfactant (CTAB) to physically prevent CNCs to interact with each other and reduce the amount of hydrogen bonding. After coupling unmodified CNCs with CTAB Fig. 5d–f, we did not notice a significant change in the morphology of CNCs, which is due to the low degree of substitution of CTAB onto CNCs. However, in the case of coupling TCNCs with



**Fig. 5** TEM images of unmodified CNCs (a–c), CNCs<sup>-CTA<sup>+</sup></sup> (d–f) and TCNCs<sup>-CTA<sup>+</sup></sup> (g–i) from aqueous suspension



CTAB, the TEM images (Fig. 5g–i), reveals a significant improvement in the distribution of the fibers as less agglomerates are observed.

#### Mechanical properties of PA6 nanocomposite thin films

PA6 nanocomposite thin films were developed after each surface modification and the associated mechanical properties were investigated at 1%, 2.5% and 5% wt.% loadings. Typical stress–strain graphs of the CNCs (a), CNCs<sup>-CTA<sup>+</sup></sup> (b), TCNCs (c) and TCNCs<sup>-CTA<sup>+</sup></sup> (d) reinforced PA6 are presented in Fig. 6.

Figure 7a–c show the elastic moduli, tensile strength, and % strain at failure of the PA6 nanocomposite thin films, respectively. The pure PA6 thin film (non-reinforced film) was used as the control to compare to the nanocomposites as CNC ratio increased. At 1% CNCs, no change in the average elastic modulus was observed, while an increase of 38% and 52% was observed for 2.5% and 5% CNCs (blue) (Fig. 7a). Modifying CNCs with CTAB resulted in a slight decrease in the elastic modulus at low wt.% loadings then a slight increase at 5 wt.%. (green). The modification of CNCs with CTAB offers no improvement

to the elastic modulus when compared to unmodified CNCs. This could be due to the low degree of substitution of CTAB onto CNCs. The small, or lack of, improvement for CNCs and CNC<sup>-CTA<sup>+</sup></sup> therefore causes weak compatibility between CNCs and PA6 and thus low stress transfer at the filler–matrix interface.

The addition of TCNCs resulted in significant improvement in the elastic modulus of the PA6 films. At 1, 2.5, and 5% TCNCs, the average elastic modulus increased by 89%, 120% and 132%, respectively. These improvements are due to the oxidation of CNCs. It is known that the mechanism behind this treatment is the selective C6 primary hydroxyl of CNCs to carboxylate groups (COO<sup>-Na<sup>+</sup></sup>). Such carboxyl groups enable greater electrostatic interactions between CNCs fibers, which promotes their dispersion in the PA6. For this reason, CNCs was oxidized to increase the surface charge density and increase interactions with CTAB thus increasing the degree of substitution. The high degree of substitution of CTAB on TCNCs results in improvement in the elastic modulus. TCNC<sup>-CTA<sup>+</sup></sup> at 1, 2.5 and 5% show an improvement of 142%, 163% and 164%, respectively. Of note, these are only slight increases when compared to the TCNCs results. However,

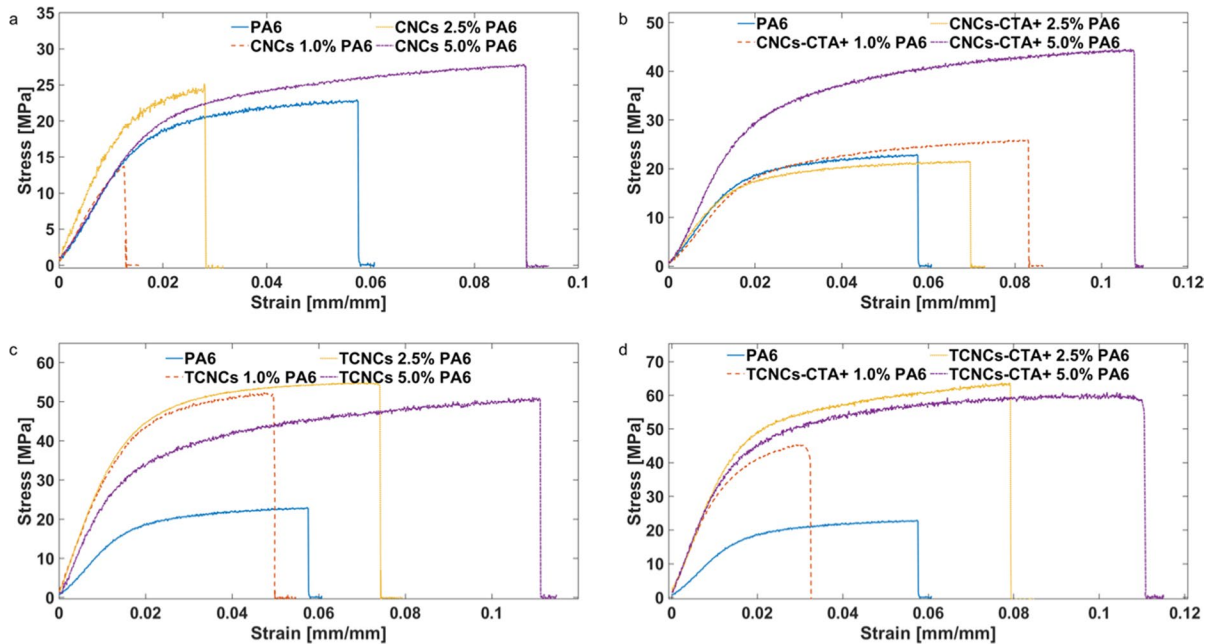


**Fig. 6** Typical stress–strain graphs of the CNCs (a), CNCs<sup>-CTA+</sup> (b), TCNCs (c) and TCNCs<sup>-CTA+</sup> (d) reinforced PA6 samples

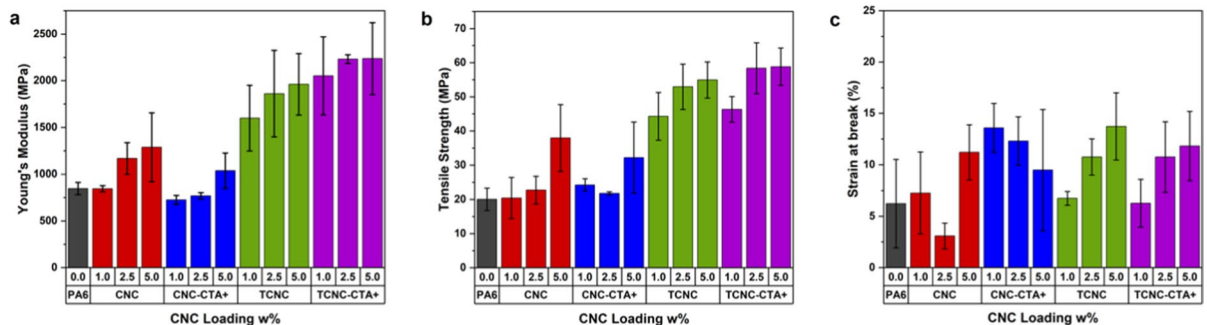


**Fig. 7** (a) young's modulus and (b) tensile strength, (c) strain at break of CNC, TCNC, CNCs<sup>-CTA+</sup> and TCNCs<sup>-CTA+</sup> reinforced PA6 nanocomposites at loading 0, 1, 2.5 and 5 wt.%

these are positive improvements in comparison to the unoxidized CNCs coupled with CTAB, which had a negative impact on the mechanical properties. We associate the improvements in elastic modulus to the increase in surface charge density and the increase in degree of substitution.

The tensile strength of PA6 nanocomposite thin films is presented in Fig. 7b. At low loadings, CNCs and CNC<sup>-CTA+</sup> show no significant improvement in tensile strength. At 5 wt.% loading, a 90% increase in tensile strength is observed when CNCs are added to PA6. CNC<sup>-CTA+</sup> also showed an improvement when

compared to PA6, however, the coupling of CTAB to the CNC surface offers no significant improvement over adding only CNCs. Again, this is attributed to the low degree of substitution, weak compatibility, and low stress transfer at the filler-matrix interface.

The oxidation of CNCs improved the tensile strength by 174% at 5 wt.% loading. Similar to the elastic modulus data, only slight improvements were observed for PA6 films with TCNC<sup>-CTA+</sup> when compared to only TCNCs. At 1, 2.5 and 5 wt.% an increase of 131%, 191% and 193%, respectively, were observed for TCNC<sup>-CTA+</sup>. The increase in

tensile strength for TCNCs and TCNC-CTA<sup>+</sup> indicates a homogeneous dispersion in PA6 and is a result of increased surface charge density and a higher degree of substitution for CTAB. The slight increase in the mechanical properties for PA6 films with TCNC-CTSA<sup>+</sup> when compared to TCNCs is probably due to the intercalation of the spacer molecule (CTAB), which moves away the fibers from each other and, consequently, makes them more dispersed within the matrix.

In order to understand the effect of modification on the properties of nanocomposites, ANOVA test along with post-hoc T-test is conducted. Table 2 shows the statistical comparison of elastic modulus, tensile strength and strain at break for each nanoparticle loading. The (<sup>a</sup>,<sup>b</sup>, and <sup>c</sup>) indicate the statistically significant differences in the data sets in each rows per reinforcing loading ( $p < 0.05$ ), as determined through one-way ANOVA analysis and post-hoc T-test. The superscripts are ordered alphabetically for each particle loading, and the largest mean comes the earliest in the alphabet.

For example, at 1.0 and 2.5% particle loading, it is observed that modification of CNC with CTA+ lowered the elastic modulus and strength significantly, while at 5.0% particle loading, this difference is not significant. The third modification, TCNC, significantly provides higher mechanical properties than CNC-CTA+ for each loading. Although the average elastic modulus and tensile strength TCNC-CTA+ reinforced PA6 is higher than TCNC at each loading, the difference is not significant. It can be concluded the best modification TCNC and TCNC-CTA+. The slight increase in the latter modification could provide higher mechanical properties as the dispersion and distribution of TCNC-CTA+ is promoted by two features: negative charges, resulting from Tempo oxidation and interactions between these negative charges and positive charges of surfactant (CTAB). This strong adhesion causes a steric hindrance because of long aliphatic chain of CTAB.

## Conclusion

The surface of CNCs were modified using TEMPO oxidation and cationic adsorption of CTAB. The modification was confirmed and characterized using FTIR, XPS, XRD, zeta potential, CHNS elemental

**Table 2** Mechanical properties of the nanocomposites

Properties	1.0%			2.5%			5.0%					
	CNC	CNC-CTA+	TCNC	TCNC-CTA+	CNC	CNC-CTA+	TCNC	TCNC-CTA+	CNC	CNC-CTA+	TCNC	TCNC-CTA+
<i>Average values</i>												
Elastic modulus (MPa)	844.8 <sup>b</sup>	725.4 <sup>c</sup>	1599.7 <sup>a</sup>	2052.5 <sup>a</sup>	1168.8 <sup>b</sup>	769.2 <sup>c</sup>	1861.3 <sup>ab</sup>	2230.8 <sup>a</sup>	1288.0 <sup>b</sup>	1037.4 <sup>b</sup>	1961.1 <sup>a</sup>	2237.1 <sup>a</sup>
Tensile strength (MPa)	20.4 <sup>b</sup>	24.3 <sup>b</sup>	44.3 <sup>a</sup>	46.3 <sup>a</sup>	22.7 <sup>b</sup>	21.8 <sup>b</sup>	52.9 <sup>a</sup>	58.4 <sup>a</sup>	38.0 <sup>b</sup>	32.2 <sup>b</sup>	54.9 <sup>a</sup>	58.8 <sup>a</sup>
Strain at break (%)	9.2 <sup>b</sup>	14.0 <sup>a</sup>	7.1 <sup>bc</sup>	6.9 <sup>c</sup>	3.1 <sup>b</sup>	12.3 <sup>a</sup>	10.8 <sup>a</sup>	10.8 <sup>a</sup>	11.2 <sup>a</sup>	9.5 <sup>b</sup>	11.0 <sup>a</sup>	11.8 <sup>a</sup>
<i>Standard deviations</i>												
Elastic modulus (MPa)	32.2	55.7	351.9	418.4	167.7	39.2	462.8	46.8	367.7	189.1	328.7	386.1
Tensile strength (MPa)	6.0	1.8	7.0	3.7	4.1	0.5	6.6	7.4	9.8	10.4	5.3	5.4
Strain at break (%)	1.0	2.7	0.1	2.4	16.1	2.4	1.8	3.4	4.6	5.9	6.8	3.1

analysis and TEM. CNC reinforced PA6 thin films were examined using mechanical strength analysis. The lack of surface charge density and degree of substitution of CTAB on non-oxidized CNCs resulted in minimal elastic modulus and tensile strength improvement. Conversely, TCNCs<sup>-</sup>CTA<sup>+</sup> showed elastic modulus and tensile strength improvements as high as 142% and 131%, respectively at only 1 wt.% loading. Work is in progress to investigate the effect of spin-coating parameters on the morphological and mechanical properties.

**Acknowledgements** The authors gratefully acknowledge the Alberta Innovates and Alberta-Ontario Innovation Program, FPInnovations (SFR02735 Nanocellulose Challenges) and Natural Science and Engineering Research Council of Canada (NSERC) Collaborative Research and Development Grants (CRDPJ 500602-16) for financial support.

**Author contributions** AB Conducting experiments, analyzing and interpreting data, manuscript writing. CR Experimental support. ECD Experimental support, manuscript editing. CA Supervising academic. MM Supervising academic.

#### Declarations

**Conflict of interest** The authors declare that they have no conflict of interest.

**Informed consent** All the authors have provided their consent for the submission of the presented work.

#### References

- Abou-Zeid RE, Hassan EA, Bettaieb F et al (2015) Use of cellulose and oxidized cellulose nanocrystals from olive stones in chitosan bionanocomposites. *J Nanomater* 2015:1–11
- Baiardo M, Frisoni G, Scandola M, Licciardello A (2002) Surface chemical modification of natural cellulose fibers. *J Appl Polym Sci* 83:38–45. <https://doi.org/10.1002/app.2229>
- Beck S, Méthot M, Bouchard J (2015) Erratum to: General procedure for determining cellulose nanocrystal sulfate half-ester content by conductometric titration. *Cellulose* 22:117. <https://doi.org/10.1007/s10570-014-0539-1>
- Ben Azouz K, Ramires EC, Van den Fonteyne W et al (2012) Simple method for the melt extrusion of a cellulose nanocrystal reinforced hydrophobic polymer. *ACS Macro Lett* 1:236–240. <https://doi.org/10.1021/mz2001737>
- Bendahou A, Hajlane A, Dufresne A et al (2015) Esterification and amidation for grafting long aliphatic chains on to cellulose nanocrystals: a comparative study. *Res Chem Intermed* 41:4293–4310. <https://doi.org/10.1007/s11164-014-1530-z>
- Benkaddour A, Jradi K, Robert S, Daneault C (2013a) Grafting of polycaprolactone on oxidized nanocelluloses by click chemistry. *Nanomaterials* 3:141–157
- Benkaddour A, Jradi K, Robert S, Daneault C (2013b) Study of the effect of grafting method on surface polarity of tempo-oxidized nanocellulose using polycaprolactone as the modifying compound: esterification versus click chemistry. *Nanomaterials* 3:638–654. <https://doi.org/10.3390/nano3040638>
- Cao X, Habibi Y, Lucia LA (2009) One-pot polymerization, surface grafting, and processing of waterborne polyurethane-cellulose nanocrystal nanocomposites. *J Mater Chem* 19:7137–7145. <https://doi.org/10.1039/B910517D>
- Çetin NS, Tingaut P, Özmen N et al (2009) Acetylation of cellulose nanowhiskers with vinyl acetate under moderate conditions. *Macromol Biosci* 9:997–1003. <https://doi.org/10.1002/mabi.200900073>
- Chakrabarty A, Teramoto Y (2018) Recent advances in nanocellulose composites with polymers: a guide for choosing partners and how to incorporate them. *Polymers* 10(5):517. <https://doi.org/10.3390/polym10050517>
- Corrêa AC, de Morais TE, Carmona VB et al (2014) Obtaining nanocomposites of polyamide 6 and cellulose whiskers via extrusion and injection molding. *Cellulose* 21:311–322. <https://doi.org/10.1007/s10570-013-0132-z>
- Eichhorn SJ (2011) Cellulose nanowhiskers: promising materials for advanced applications. *Soft Matter* 7:303–315. <https://doi.org/10.1039/C0SM00142B>
- French AD (2014) Idealized powder diffraction patterns for cellulose polymorphs. *Cellulose* 21:885–896. <https://doi.org/10.1007/s10570-013-0030-4>
- Gardner DJ, Oporto GS, Mills R, Samir MASA (2008) Adhesion and surface issues in cellulose and nanocellulose. *J Adhes Sci Technol* 22:545–567. <https://doi.org/10.1163/156856108X295509>
- Gradwell SE, Rennecker S, Esker AR et al (2004) Surface modification of cellulose fibers: towards wood composites by biomimetics. *CR Biol* 327:945–953. <https://doi.org/10.1016/j.crv.2004.07.015>
- Heera M, D CE (2014) Surface modification of cellulose nanocrystals with cetyltrimethylammonium bromide. *Nord Pulp Pap Res J* 29:46
- Isogai A, Saito T, Fukuzumi H (2011) TEMPO-oxidized cellulose nanofibers. *Nanoscale* 3:71–85. <https://doi.org/10.1039/C0NR00583E>
- Jordan JH, Easson MW, Condon BD (2019) Alkali hydrolysis of sulfated cellulose nanocrystals: optimization of reaction conditions and tailored surface charge. *Nanomaterials* (basel, Switzerland) 9:1232. <https://doi.org/10.3390/nano9091232>
- Kaboorani A, Riedl B (2015) Surface modification of cellulose nanocrystals (CNC) by a cationic surfactant. *Ind Crops Prod* 65:45–55. <https://doi.org/10.1016/j.indcrop.2014.11.027>
- Kalia S, Kaith BS, Kaur I (2009) Pretreatments of natural fibers and their application as reinforcing material in polymer composites—a review. *Polym Eng Sci* 49:1253–1272. <https://doi.org/10.1002/pen.21328>
- Karimi S (2017) Thermoplastic cellulose nanocomposites. handbook of nanocellulose and cellulose nanocomposites

- Khili F, Borges J, Almeida PL et al (2019) Extraction of cellulose nanocrystals with structure I and II and their applications for reduction of graphene oxide and nanocomposite elaboration. *Waste Biomass Valoriz* 10:1913–1927. <https://doi.org/10.1007/s12649-018-0202-4>
- Liimatainen H, Visanko M, Sirviö JA et al (2012) Enhancement of the nanofibrillation of wood cellulose through sequential periodate-chlorite oxidation. *Biomacromol* 13:1592–1597. <https://doi.org/10.1021/bm300319m>
- Lin N, Dufresne A (2014) Surface chemistry, morphological analysis and properties of cellulose nanocrystals with gradiented sulfation degrees. *Nanoscale* 6:5384–5393. <https://doi.org/10.1039/C3NR06761K>
- Lin N, Huang J, Dufresne A (2012) Preparation, properties and applications of polysaccharide nanocrystals in advanced functional nanomaterials: a review. *Nanoscale* 4:3274–3294. <https://doi.org/10.1039/C2NR30260H>
- Liu Y, Li M, Qiao M et al (2017) Antibacterial membranes based on chitosan and quaternary ammonium salts modified nanocrystalline cellulose. *Polym Adv Technol* 28:1629–1635. <https://doi.org/10.1002/pat.4032>
- Ljungberg N, Bonini C, Bortolussi F et al (2005) New nanocomposite materials reinforced with cellulose whiskers in atactic polypropylene: effect of surface and dispersion characteristics. *Biomacromol* 6:2732–2739. <https://doi.org/10.1021/bm050222v>
- Morandi G, Heath L, Thielemans W (2009) Cellulose nanocrystals grafted with polystyrene chains through surface-initiated atom transfer radical polymerization (SI-ATRP). *Langmuir* 25:8280–8286. <https://doi.org/10.1021/la900452a>
- Nagalakshmaiah M, El Kissi N, Dufresne A (2016) Ionic compatibilization of cellulose nanocrystals with quaternary ammonium salt and their melt extrusion with polypropylene. *ACS Appl Mater Interfaces* 8:8755–8764. <https://doi.org/10.1021/acsami.6b01650>
- Patiño-Masó J, Serra-Parareda F, Tarrés Q et al (2019) TEMPO-oxidized cellulose nanofibers: a potential bio-based superabsorbent for diaper production. *Nanomaterials* 9:1271
- Peng Y, Gardner DJ, Han Y (2015) Characterization of mechanical and morphological properties of cellulose reinforced polyamide 6 composites. *Cellulose* 22:3199–3215. <https://doi.org/10.1007/s10570-015-0723-y>
- Qua EH, Hornsby PR (2011) Preparation and characterisation of nanocellulose reinforced polyamide-6. *Plast Rubber Compos* 40:300–306. <https://doi.org/10.1179/1743289810Y.0000000019>
- Rehman N, Bica CID, de Miranda MIG, Rosa SML (2017) Dynamics of cellulose nanocrystals in the presence of hexadecyltrimethylammonium bromide. *Macromol Res* 25:767–771. <https://doi.org/10.1007/s13233-017-5089-6>
- Roman M, Winter WT (2004) Effect of sulfate groups from sulfuric acid hydrolysis on the thermal degradation behavior of bacterial cellulose. *Biomacromol* 5:1671–1677. <https://doi.org/10.1021/bm034519+>
- Saito T, Nishiyama Y, Putaux J-L et al (2006) Homogeneous suspensions of individualized microfibrils from TEMPO-catalyzed oxidation of native cellulose. *Biomacromol* 7:1687–1691. <https://doi.org/10.1021/bm060154s>
- Saito T, Kuramae R, Wohlert J et al (2013) An ultrastrong nanofibrillar biomaterial: the strength of single cellulose nanofibrils revealed via sonication-induced fragmentation. *Biomacromol* 14:248–253. <https://doi.org/10.1021/bm301674e>
- Salajková M, Berglund LA, Zhou Q (2012) Hydrophobic cellulose nanocrystals modified with quaternary ammonium salts. *J Mater Chem* 22:19798–19805. <https://doi.org/10.1039/C2JM34355J>
- Sehaqui H, Zhou Q, Ikkala O, Berglund LA (2011) Strong and tough cellulose nanopaper with high specific surface area and porosity. *Biomacromol* 12:3638–3644. <https://doi.org/10.1021/bm2008907>
- Yalcinkaya EE, Puglia D, Fortunati E et al (2017) Cellulose nanocrystals as templates for cetyltrimethylammonium bromide mediated synthesis of Ag nanoparticles and their novel use in PLA films. *Carbohydr Polym* 157:1557–1567. <https://doi.org/10.1016/j.carbpol.2016.11.038>
- Yao X, Qi X, He Y et al (2014) Simultaneous reinforcing and toughening of polyurethane via grafting on the surface of microfibrillated cellulose. *ACS Appl Mater Interfaces* 6:2497–2507. <https://doi.org/10.1021/am4056694>
- Yi J, Xu Q, Zhang X, Zhang H (2008) Chiral-nematic self-ordering of rodlike cellulose nanocrystals grafted with poly(styrene) in both thermotropic and lyotropic states. *Polymer* 49:4406–4412. <https://doi.org/10.1016/j.polymer.2008.08.008>
- Yin Y, Hong Z, Tian X et al (2018) Cellulose nanocrystals modified with quaternary ammonium salts and its reinforcement of polystyrene. *Polym Bull* 75:2151–2166. <https://doi.org/10.1007/s00289-017-2131-y>
- Yousefian H, Rodrigue D (2014) Effect of nanocrystalline cellulose on morphological, thermal, and mechanical properties of Nylon 6 composites. *Polym Compos* 37:1473–1479. <https://doi.org/10.1002/pc.23316>
- Zainuddin N, Ahmad I, Kargazadeh H, Ramli S (2017) Hydrophobic kenaf nanocrystalline cellulose for the binding of curcumin. *Carbohydr Polym* 163:261–269. <https://doi.org/10.1016/j.carbpol.2017.01.036>

**Publisher's Note** Springer Nature remains neutral with regard to jurisdictional claims in published maps and institutional affiliations.

Springer Nature or its licensor (e.g. a society or other partner) holds exclusive rights to this article under a publishing agreement with the author(s) or other rightsholder(s); author self-archiving of the accepted manuscript version of this article is solely governed by the terms of such publishing agreement and applicable law.